

# NAND gate response in a mesoscopic ring: An exact study

Santanu K. Maiti<sup>1,2,\*</sup>

<sup>1</sup>*Theoretical Condensed Matter Physics Division, Saha Institute of Nuclear Physics,  
1/AF, Bidhannagar, Kolkata-700 064, India*

<sup>2</sup>*Department of Physics, Narasinha Dutt College, 129, Belilious Road, Howrah-711 101, India*

## Abstract

NAND gate response in a mesoscopic ring threaded with a magnetic flux  $\phi$  is investigated by using Green's function formalism. The ring is attached symmetrically to two semi-infinite one-dimensional metallic electrodes and two gate voltages, namely,  $V_a$  and  $V_b$ , are applied in one arm of the ring those are treated as the two inputs of the NAND gate. We use a simple tight-binding model to describe the system and numerically compute the conductance-energy and current-voltage characteristics as functions of the gate voltages, ring-to-electrode coupling strength and magnetic flux. Our theoretical study shows that, for  $\phi = \phi_0/2$  ( $\phi_0 = ch/e$ , the elementary flux-quantum) a high output current (1) (in the logical sense) appears if one or both the inputs to the gate are low (0), while if both the inputs to the gate are high (1), a low output current (0) appears. It clearly exhibits the NAND gate behavior and this feature may be utilized in designing an electronic logic gate.

**PACS No.:** 73.23.-b; 73.63.Rt.

**Keywords:** Mesoscopic ring; Conductance;  $I$ - $V$  characteristic; NAND gate.

\***Corresponding Author:** Santanu K. Maiti  
Electronic mail: santanu.maiti@saha.ac.in

# 1 Introduction

Electronic transport in quantum confined geometries has attracted much attention since these simple looking systems are the promising building blocks for designing nanodevices especially in electronic as well as spintronic engineering. A mesoscopic metallic ring is one such promising example where electronic motion is restricted. The recent progress in nanoscience and technology has allowed us to investigate the electron transport through a mesoscopic ring in a very tunable way. Using a mesoscopic ring we can make a device that can act as a logic gate, which may be used in nano-electronic circuits. To explore this phenomenon we design a bridge system where the ring is attached to two external electrodes, so-called the electrode-ring-electrode bridge. The ring is then subjected to a magnetic flux  $\phi$ , so-called the Aharonov-Bohm (AB) flux which is the key controlling factor for the whole logical operation in this particular geometry. The theoretical description of electron transport in a bridge system has got much progress following the pioneering work of Aviram and Ratner [1]. Later, many excellent experiments [2, 3, 4] have been done in several bridge systems to understand the basic mechanisms underlying the electron transport. Though in literature both theoretical [5, 6, 7, 8, 9, 10, 11, 12, 13] as well as experimental [2, 3, 4] works on electron transport are available, yet lot of controversies are still present between the theory and experiment, and the complete knowledge of the conduction mechanism in this scale is not very well established even today. The interface geometry between the ring and the electrodes significantly controls the electronic transport in the ring. By changing the geometry, one can tune the transmission probability of an electron across the ring which is solely due to the effect of quantum interference among the electronic waves passing through different arms of the ring. Furthermore, the electron transport in the ring can be modulated in other way by tuning the magnetic flux, that threads the ring. The AB flux threading the ring may change the phases of the wave functions propagating along the different arms of the ring leading to constructive or destructive interferences, and therefore, the transmission amplitude changes [14, 15, 16, 17, 18]. Beside these factors, ring-to-electrode coupling is another important issue that controls the electron transport in a meaningful way [18]. All these are the key factors which regulate the electron transmission in the

electrode-ring-electrode bridge system and these effects have to be taken into account properly to reveal the transport mechanisms.

The main focus of the present work is to describe the NAND gate response in a mesoscopic ring threaded by a magnetic flux  $\phi$ . The ring is contacted symmetrically to the electrodes, and the two gate voltages  $V_a$  and  $V_b$  are applied in one arm of the ring (see Fig. 1) those are treated as the two inputs of the NAND gate. A simple tight-binding model is used to describe the system and all the calculations are done numerically. Here we address the NAND gate behavior by studying the conductance-energy and current-voltage characteristics as functions of the ring-electrodes coupling strengths, magnetic flux and gate voltages. Our study reveals that for a particular value of the magnetic flux,  $\phi = \phi_0/2$ , a high output current (1) (in the logical sense) is available if one or both the inputs to the gate are low (0), while if both the inputs to the gate are high (1), a low output current (0) appears. This phenomenon clearly shows the NAND gate behavior. To the best of our knowledge the NAND gate response in such a simple system has yet not been addressed in the literature.

The scheme the paper is as follow. Following the introduction (Section 1), in Section 2, we described the model and the theoretical formulations for the calculation. Section 3 explores the results, and finally, we conclude our study in Section 4.

## 2 Model and the synopsis of the theoretical background

Let us begin by referring to Fig. 1. A mesoscopic ring, threaded by a magnetic flux  $\phi$ , is attached symmetrically (upper and lower arms have equal number of lattice points) to two semi-infinite one-dimensional (1D) metallic electrodes. The atoms  $a$  and  $b$  in the upper arm of the ring are subjected to the gate voltages  $V_a$  and  $V_b$ , respectively, those are treated as the two inputs of the NAND gate. On the other hand, two additional voltages  $V_\alpha$  and  $V_\beta$  are applied in the atoms  $\alpha$  and  $\beta$ , respectively, in the lower arm of the ring.

At very low temperature and bias voltage the conductance  $g$  of the ring can be expressed from the Landauer conductance formula [19, 20],

$$g = \frac{2e^2}{h}T \quad (1)$$

where  $T$  gives the transmission probability of an

electron across the ring. This ( $T$ ) can be represented in terms of the Green's function of the ring and its coupling to the two electrodes by the relation [19, 20],

$$T = \text{Tr} [\Gamma_S G_R^r \Gamma_D G_R^a] \quad (2)$$

where  $G_R^r$  and  $G_R^a$  are respectively the retarded and advanced Green's functions of the ring including the effects of the electrodes. Here  $\Gamma_S$  and  $\Gamma_D$  describe the coupling of the ring to the source and drain, respectively. For the complete system i.e., the ring, source and drain, the Green's function is defined as,

$$G = (E - H)^{-1} \quad (3)$$

where  $E$  is the injecting energy of the source electron. To Evaluate this Green's function, the inversion of an infinite matrix is needed since the complete system consists of the finite ring and the two semi-infinite electrodes. However, the entire system

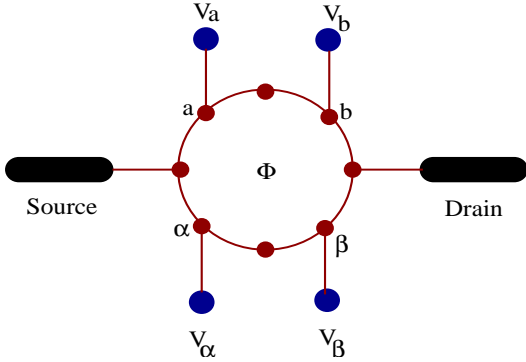


Figure 1: (Color online). Schematic representation for the operation of a NAND gate. The atoms  $a$ ,  $b$ ,  $\alpha$  and  $\beta$  are subjected to the voltages  $V_a$ ,  $V_b$ ,  $V_\alpha$  and  $V_\beta$ , respectively, those are variable.

can be partitioned into sub-matrices corresponding to the individual sub-systems and the Green's function for the ring can be effectively written as,

$$G_R = (E - H_R - \Sigma_S - \Sigma_D)^{-1} \quad (4)$$

where  $H_R$  is the Hamiltonian of the ring that can be expressed within the non-interacting picture like,

$$H_R = \sum_i (\epsilon_{i0} + V_a \delta_{ia} + V_b \delta_{ib} + V_\alpha \delta_{i\alpha} + V_\beta \delta_{i\beta}) + \sum_{\langle ij \rangle} t (c_i^\dagger c_j e^{i\theta} + h.c.) \quad (5)$$

In this Hamiltonian  $\epsilon_{i0}$ 's are the site energies for all the sites  $i$  except the sites  $i = a, b, \alpha$  and  $\beta$  where

the gate voltages  $V_a$ ,  $V_b$ ,  $V_\alpha$  and  $V_\beta$  are applied, those are variable. These gate voltages can be incorporated through the site energies as expressed in the above Hamiltonian.  $c_i^\dagger$  ( $c_i$ ) is the creation (annihilation) operator of an electron at the site  $i$  and  $t$  is the nearest-neighbor hopping integral. The phase factor  $\theta = 2\pi\phi/N\phi_0$  comes due to the flux  $\phi$  threaded by the ring, where  $N$  corresponds to the total number of atomic sites in the ring. In Eq. (4),  $\Sigma_S = h_{SR}^\dagger g_S h_{SR}$  and  $\Sigma_D = h_{DR} g_D h_{DR}^\dagger$  are the self-energy operators due to the two electrodes, where  $g_S$  and  $g_D$  are the Green's functions for the source and drain, respectively.  $h_{SR}$  and  $h_{DR}$  are the coupling matrices and they will be non-zero only for the adjacent points of the ring and the electrodes as shown in Fig. 1. The coupling terms  $\Gamma_S$  and  $\Gamma_D$  for the ring can be calculated through the expression [19, 21],

$$\Gamma_{S(D)} = i \left[ \Sigma_{S(D)}^r - \Sigma_{S(D)}^a \right] \quad (6)$$

where  $\Sigma_{S(D)}^r$  and  $\Sigma_{S(D)}^a$  are the retarded and advanced self-energies, respectively, and they are conjugate to each other. Datta *et al.* [19, 21] have shown that the self-energies can be expressed like as,

$$\Sigma_{S(D)}^r = \Lambda_{S(D)} - i\Delta_{S(D)} \quad (7)$$

where  $\Lambda_{S(D)}$  are the real parts of the self-energies which correspond to the shift of the energy eigenvalues of the ring, and the imaginary parts  $\Delta_{S(D)}$  of the self-energies represent the broadening of these energy levels. This broadening is much larger than the thermal broadening, and accordingly, we restrict our all calculations only at absolute zero temperature. These two self-energies  $\Sigma_S$  and  $\Sigma_D$  bear all the information of the coupling of the ring to the source and drain, respectively [19]. A similar kind of tight-binding Hamiltonian is also used, except the phase factor  $\theta$ , to describe the 1D perfect electrodes where the Hamiltonian is parametrized by constant on-site potential  $\epsilon_0$  and nearest-neighbor hopping integral  $t_0$ . The hopping integral between the source and the ring is  $\tau_S$ , while it is  $\tau_D$  between the ring and the drain.

The current  $I$  passing through the ring is depicted as a single-electron scattering process between the two reservoirs of charge carriers. The current-voltage relation is evaluated from the following expression [19],

$$I(V) = \frac{e}{\pi\hbar} \int_{E_F - eV/2}^{E_F + eV/2} T(E, V) dE \quad (8)$$

where  $E_F$  is the equilibrium Fermi energy. Here we assume that the entire voltage is dropped across the ring-electrode interfaces, and it is examined that under such an assumption the  $I$ - $V$  characteristics do not change their qualitative features.

All the results in this communication are determined at absolute zero temperature, but they should valid even for finite temperature ( $\sim 300$  K), since the broadening of the energy levels of the ring due to its coupling to the electrodes becomes much larger than that of the thermal broadening [19]. For simplicity, we take the unit  $c = e = h = 1$  in our present calculation.

### 3 Results and discussion

Let us start our discussion by mentioning the values of the different parameters used for the numerical calculation. In the ring, the on-site energy  $\epsilon_{i0}$

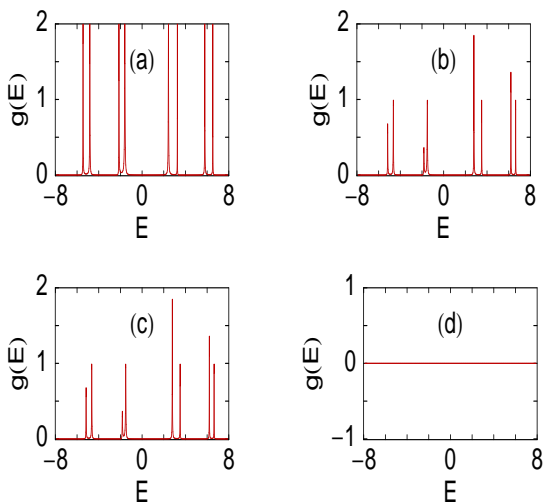


Figure 2: (Color online).  $g$ - $E$  curves in the weak-coupling limit for a mesoscopic ring with  $N = 8$ ,  $V_\alpha = V_\beta = 2$  and  $\phi = 0.5$ . (a)  $V_a = V_b = 0$ , (b)  $V_a = 2$  and  $V_b = 0$ , (c)  $V_a = 0$  and  $V_b = 2$  and (d)  $V_a = V_b = 2$ .

taken as 0 for all the sites  $i$ , except the sites  $i = a, b, \alpha$  and  $\beta$  where the site energies are taken as  $V_a, V_b, V_\alpha$  and  $V_\beta$  respectively, and the nearest-neighbor hopping strength  $t$  is set to 3. On the other hand, for the side attached electrodes the on-site energy ( $\epsilon_0$ ) and the nearest-neighbor hopping strength ( $t_0$ ) are fixed to 0 and 4, respectively. The voltages  $V_\alpha$  and  $V_\beta$  are set to 2 and the Fermi energy  $E_F$  is set at 0. Throughout the study, we focus our

results for the two limiting cases depending on the strength of the coupling of the ring to the source and drain. In one case we use the condition  $\tau_{S(D)} \ll t$ , which is so-called the weak-coupling limit. For this regime we choose  $\tau_S = \tau_D = 0.5$ . In the other case the condition  $\tau_{S(D)} \sim t$  is used, which is named as the strong-coupling limit. In this particular regime, the values of the parameters are set as  $\tau_S = \tau_D = 2.5$ . The key controlling parameter for all these calculations is the magnetic flux  $\phi$  which is set to  $\phi_0/2$  i.e., 0.5 in our chosen unit.

Figure 2 shows the variation of the conductance ( $g$ ) as a function of the injecting electron energy ( $E$ ) in the limit of weak-coupling for a mesoscopic

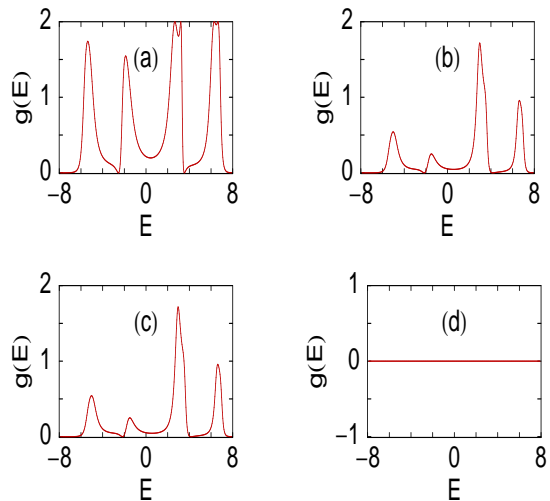


Figure 3: (Color online).  $g$ - $E$  curves in the strong-coupling limit for a mesoscopic ring with  $N = 8$ ,  $V_\alpha = V_\beta = 2$  and  $\phi = 0.5$ . (a)  $V_a = V_b = 0$ , (b)  $V_a = 2$  and  $V_b = 0$ , (c)  $V_a = 0$  and  $V_b = 2$  and (d)  $V_a = V_b = 2$ .

ring with  $N = 8$  and  $V_\alpha = V_\beta = 2$ , where (a), (b), (c) and (d) correspond to the results for the different values of  $V_a$  and  $V_b$ . When both the two inputs  $V_a$  and  $V_b$  are identical to 2 i.e., both the inputs are high, the conductance  $g$  becomes exactly zero (Fig. 2(d)) for all energies. This reveals that the electron cannot conduct from the source to the drain through the ring. While, for the cases where anyone or both the inputs to the gate are zero (low), the conductance shows fine resonant peaks for some particular energies, as shown in Figs. 2(a), (b) and (c), respectively. Thus, in all these three cases, the electron can conduct through the ring. From Fig. 2(a) it is observed that, at the resonances the conductance  $g$  approaches the value 2, and ac-

cordingly, the transmission probability  $T$  becomes unity, since the expression  $g = 2T$  is satisfied from the Landauer conductance formula (see Eq. 1 with  $e = h = 1$ ). The height of the resonant peaks gets down ( $T < 1$ ) for the cases where anyone of the two inputs is high and other is low (Figs. 2(b) and (c)). All these resonant peaks are associated with the energy eigenvalues of the ring, and thus, it can be predicted that the conductance spectrum manifests itself the electronic structure of the ring. This

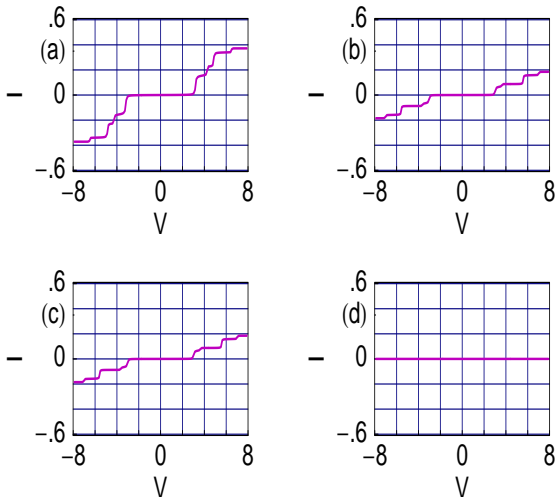


Figure 4: (Color online).  $I$ - $V$  curves in the weak-coupling limit for a mesoscopic ring with  $N = 8$ ,  $V_\alpha = V_\beta = 2$  and  $\phi = 0.5$ . (a)  $V_a = V_b = 0$ , (b)  $V_a = 2$  and  $V_b = 0$ , (c)  $V_a = 0$  and  $V_b = 2$  and (d)  $V_a = V_b = 2$ .

reveals that more resonant peaks are expected for the larger rings, associated with their energy spectra. Now we illustrate the dependences of the gate voltages on the electron transport for these four different cases. The probability amplitude of getting an electron across the ring depends on the quantum interference of the electronic waves passing through the two arms (upper and lower) of the ring. For the symmetrically connected ring i.e., when the two arms of the ring become identical with each other, the probability amplitude is exactly zero ( $T = 0$ ) for the flux  $\phi = \phi_0/2$ . This is due to the result of the quantum interference among the two waves in the two arms of the ring, which can be obtained in a very simple mathematical calculation. So, for the case when both the two inputs to the gate are identical to 2 i.e.,  $V_a = V_b = 2$ , the upper and lower arms of the ring become exactly similar. This is due to the fact that the potentials  $V_\alpha$  and  $V_\beta$  are

also fixed to 2. Therefore, in this particular case the transmission probability drops to zero. If the two inputs  $V_a$  and  $V_b$  are different from the potentials applied in the sites  $\alpha$  and  $\beta$ , then the two arms are no longer identical to each other and the transmission probability will not vanish. Hence, to get the zero transmission probability when both the inputs are high, we should tune  $V_\alpha$  and  $V_\beta$  properly, observing the input potentials and vice versa. On the other hand, due to the breaking of the symmetry of the two arms (i.e., two arms are no longer identical to each other) in the other three cases by making anyone or both the two inputs to the gate are zero (low), the non-zero value of the transmission probability is achieved which reveals the electron conduc-

Table 1: NAND gate behavior in the limit of weak-coupling. The current  $I$  is computed at the bias voltage 6.02.

Input-I ( $V_a$ )	Input-II ( $V_b$ )	Current ( $I$ )
0	0	0.339
2	0	0.157
0	2	0.157
2	2	0

tion across the ring. The reduction of the transmission probability from unity for the cases where any one of the two gates is high and other is low compared to the case where both the gates are low is solely due to the quantum interference effect. Thus it can be emphasized that the electron conduction takes place across the ring if any one or both the inputs to the gate are low, while if both the inputs are high, the conduction is no longer possible. This feature clearly describes the NAND gate behavior. In this context we also discuss the effect of the ring-to-electrode coupling. As illustrative examples, in Fig. 3 we show the conductance-energy characteristics for the strong-coupling limit, where (a), (b), (c) and (d) are drawn respectively for the same gate voltages as in Fig. 2. In the strong-coupling case, all the resonant peaks get substantial widths compared to the weak-coupling case. This is due to the broadening of the energy levels of the ring in the limit of strong coupling, where the contribution comes from the imaginary parts of the self-energies  $\Sigma_S$  and  $\Sigma_D$ , respectively [19]. Therefore, by tuning the coupling strength, we can get the electron transmission across the ring for the wider range of energies and it provides an important behavior in

the study of current-voltage ( $I$ - $V$ ) characteristics.

All these properties of electron transfer can be much more clearly understood from our presented current-voltage ( $I$ - $V$ ) characteristics. The current across the ring is determined by integrating the transmission function  $T$  as prescribed in Eq. 8. The transmission function varies exactly similar to that of the conductance spectrum, differ only in magnitude by the factor 2 since the relation  $g = 2T$  holds from the Landauer conductance formula Eq. 1. As representative examples, in Fig. 4 we plot the  $I$ - $V$  characteristics for a mesoscopic ring with  $N = 8$  in the limit of weak-coupling, where (a), (b), (c)

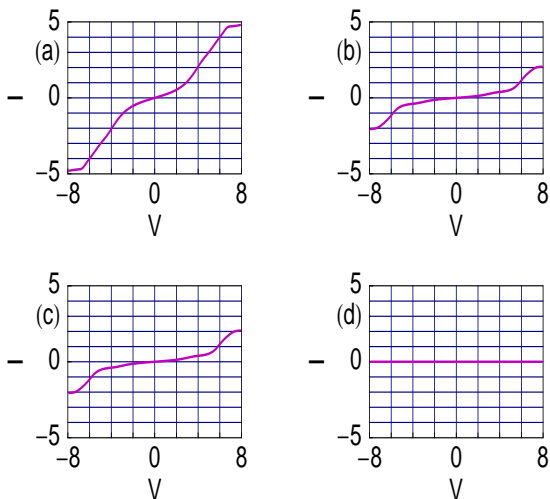


Figure 5: (Color online).  $I$ - $V$  curves in the strong-coupling limit for a mesoscopic ring with  $N = 8$ ,  $V_\alpha = V_\beta = 2$  and  $\phi = 0.5$ . (a)  $V_a = V_b = 0$ , (b)  $V_a = 2$  and  $V_b = 0$ , (c)  $V_a = 0$  and  $V_b = 2$  and (d)  $V_a = V_b = 2$ .

and (d) correspond to the results for the different cases of the input voltages. Quite interestingly we see that when both the two inputs to the gate are identical to 2 (high), the current  $I$  becomes zero (see Fig. 4(d)) for the entire bias voltage  $V$ . This feature is clearly understood from the conductance spectrum, Fig. 2(d), since the current is computed from the integration method of the transmission function  $T$ . In all the other three cases of the input voltages, a non-zero value of the current is obtained, those are clearly presented in Figs. 4(a), (b) and (c). These figures show that the current exhibits staircase-like structure with fine steps as a function of the applied bias voltage. This is due to the existence of the fine resonant peaks in the conductance spectra in the weak-coupling limit. With the increase

of the bias voltage  $V$ , the electrochemical potentials on the electrodes are shifted gradually, and finally cross one of the quantized energy levels of the ring. Accordingly, a current channel is opened up which provides a jump in the  $I$ - $V$  characteristic curve. Here, it is also important to mention that the non-zero value of the current appears beyond a finite value of the bias voltage  $V$ , so-called the threshold voltage ( $V_{th}$ ). This  $V_{th}$  can be changed by controlling the size ( $N$ ) of the ring. From these current-voltage curves, the NAND gate behavior of the ring can be observed very nicely. To make it much clear, in Table 1, we show a quantitative estimate of the typical current amplitude determined at the bias voltage  $V = 6.02$ . It is observed that, when any one of the two gates is high and other is low, the current gets the value 0.157, and for

Table 2: NAND gate behavior in the limit of strong-coupling. The current  $I$  is computed at the bias voltage 6.02.

Input-I ( $V_a$ )	Input-II ( $V_b$ )	Current ( $I$ )
0	0	4.018
2	0	1.174
0	2	1.174
2	2	0

the case when both the two inputs are low, it ( $I$ ) achieves the value 0.339. While, for the case when both the two inputs are high ( $V_a = V_b = 2$ ), the current becomes exactly zero. In the same footing, as above, here we also describe the  $I$ - $V$  characteristics for the strong-coupling limit. In this limit, the current varies almost continuously with the applied bias voltage and gets much larger amplitude than the weak-coupling case as presented in Fig. 5. The reason is that, in the limit of strong-coupling all the energy levels get broadened which provide larger current in the integration procedure of the transmission function  $T$ . Thus by tuning the strength of the ring-to-electrode coupling, we can achieve very large current amplitude from the very low one for the same bias voltage  $V$ . All the other properties i.e., the dependences of the gate voltages on the  $I$ - $V$  characteristics are exactly similar to those as given in Fig. 4. In this strong-coupling limit we also make a quantitative study for the typical current amplitude, given in Table 2, where the current amplitude is determined at the same bias voltage ( $V = 6.02$ ) as earlier. The response of the output current is

exactly similar to that as given in Table 1. Here the current achieves the value 1.174 in the cases where any one of the two gates is high and other is low, and it ( $I$ ) becomes 4.018 for the case where both the two inputs are low. On the other hand, the current becomes exactly zero for the case where  $V_a = V_b = 2$ . The non-zero values of the current in this strong-coupling limit are much larger than the weak-coupling case, as expected. From these results we can clearly manifest that a mesoscopic ring exhibits the NAND gate response.

## 4 Concluding remarks

In this work, we have explored the NAND gate response in a mesoscopic metallic ring threaded by a magnetic flux  $\phi$  in the Green's function formalism. The ring is attached symmetrically to the electrodes and two gate voltages  $V_a$  and  $V_b$  are applied in one arm of the ring those are taken as the two inputs of the NAND gate. A simple tight-binding model is used to describe the system and all the calculations are exact and performed numerically. We have computed the conductance-energy and current-voltage characteristics as functions of the gate voltages, ring-to-electrode coupling strength and magnetic flux. Very interestingly we have observed that, for the half flux-quantum value of  $\phi$  ( $\phi = \phi_0/2$ ), a high output current (1) (in the logical sense) appears if one or both the inputs to the gate are low (0). On the other hand, if both the inputs to the gate are high (1), a low output current (0) appears. It clearly manifests the NAND gate behavior and this aspect may be utilized in designing a tailor made electronic logic gate.

Throughout our work, we have addressed the conductance-energy and current-voltage characteristics for a quantum ring with total number of atomic sites  $N = 8$ . In our model calculations, this typical number ( $N = 8$ ) is chosen only for the sake of simplicity. Here it is important to note that for a larger ring with more atomic sites, one can also apply input voltages to the other atomic sites, preserving the symmetry between the upper and lower arms of the ring. Though the results presented here change numerically with the ring size ( $N$ ) and the distance between the input positions, but all the basic features remain exactly invariant since the results solely depend on the quantum interference effect of the electronic waves passing through the two arms of the ring. To be more specific, it is important to note that, in real situation the experimentally achievable rings have typical diameters within

the range 0.4-0.6  $\mu\text{m}$ . In such a small ring, unrealistically very high magnetic fields are required to produce a quantum flux. To overcome this situation, Hod *et al.* have studied extensively and proposed how to construct nanometer scale devices, based on Aharonov-Bohm interferometry, those can be operated in moderate magnetic fields [22, 23, 24, 25].

In the present paper we have done all the calculations by ignoring the effects of the temperature, electron-electron correlation, disorder, etc. Due to these factors, any scattering process that appears in the arms of the rings would have influence on electronic phases, and, in consequences can disturb the quantum interference effects. Here we have assumed that, in our sample all these effects are too small, and accordingly, we have neglected all these factors in this particular study.

The importance of this article is concerned with (i) the simplicity of the geometry and (ii) the smallness of the size. To the best of our knowledge the NAND gate response in such a simple low-dimensional system that can be operated even at finite temperature ( $\sim 300$  K) has not been addressed earlier in the literature.

## References

- [1] A. Aviram and M. Ratner, Chem. Phys. Lett. **29**, 277 (1974).
- [2] J. Chen, M. A. Reed, A. M. Rawlett and J. M. Tour, Science **286**, 1550 (1999).
- [3] M. A. Reed, C. Zhou, C. J. Muller, T. P. Burgin and J. M. Tour, Science **278**, 252 (1997).
- [4] T. Dadoosh, Y. Gordin, R. Krahne, I. Khivrich, D. Mahalu, V. Frydman, J. Sperling, A. Yacoby and I. Bar-Joseph, Nature **436**, 677 (2005).
- [5] A. Nitzan, Annu. Rev. Phys. Chem. **52**, 681 (2001).
- [6] A. Nitzan and M. A. Ratner, Science **300**, 1384 (2003).
- [7] P. A. Orellana, M. L. Ladron de Guevara, M. Pacheco and A. Latge, Phys. Rev. B **68**, 195321 (2003).
- [8] P. A. Orellana, F. Dominguez-Adame, I. Gomez and M. L. Ladron de Guevara, Phys. Rev. B **67**, 085321 (2003).

- [9] V. Mujica, M. Kemp and M. A. Ratner, J. Chem. Phys. **101**, 6849 (1994).
- [10] V. Mujica, M. Kemp, A. E. Roitberg and M. A. Ratner, J. Chem. Phys. **104**, 7296 (1996).
- [11] K. Walczak, Phys. Stat. Sol. (b) **241**, 2555 (2004).
- [12] K. Walczak, arXiv:0309666.
- [13] W. Y. Cui, S. Z. Wu, G. Jin, X. Zhao and Y. Q. Ma, Eur. Phys. J. B. **59**, 47 (2007).
- [14] R. Baer and D. Neuhauser, J. Am. Chem. Soc. **124**, 4200 (2002).
- [15] D. Walter, D. Neuhauser and R. Baer, Chem. Phys. **299**, 139 (2004).
- [16] K. Tagami, L. Wang and M. Tsukada, Nano Lett. **4**, 209 (2004).
- [17] K. Walczak, Cent. Eur. J. Chem. **2**, 524 (2004).
- [18] R. Baer and D. Neuhauser, Chem. Phys. **281**, 353 (2002).
- [19] S. Datta, *Electronic transport in mesoscopic systems*, Cambridge University Press, Cambridge (1997).
- [20] M. B. Nardelli, Phys. Rev. B **60**, 7828 (1999).
- [21] W. Tian, S. Datta, S. Hong, R. Reifengerger, J. I. Henderson and C. I. Kubiak, J. Chem. Phys. **109**, 2874 (1998).
- [22] O. Hod, R. Baer and E. Rabani, J. Phys. Chem. B **108**, 14807 (2004).
- [23] O. Hod, R. Baer and E. Rabani, J. Phys.: Condens. Matter **20**, 383201 (2008).
- [24] O. Hod, R. Baer and E. Rabani, J. Am. Chem. Soc. **127**, 1648 (2005).
- [25] O. Hod, E. Rabani and R. Baer, Acc. Chem. Res. **39**, 109 (2006).